Molecular Catalysis 540 (2023) 113049

Contents lists available at ScienceDirect

Molecular Catalysis

journal homepage: www.journals.elsevier.com/molecular-catalysis

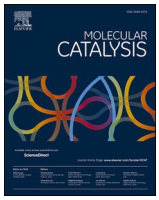

Solvent-free selective oxidation of benzyl alcohol using Ru loaded ceria-zirconia catalysts

Eleonora Aneggi [a,*], Filippo Campagnolo [a], Jacopo Segato [a], Daniele Zuccaccia [a], Walter Baratta [a], Jordi Llorca [b], Alessandro Trovarelli [c]

[a] Dipartimento di Scienze Agroalimentari, Ambientali e Animali, Sezione di Chimica, Università di Udine, Udine, Italy
[b] Institute of Energy Technologies, Department of Chemical Engineering and Barcelona Research Center in Multiscale Science and Engineering, Universitat Politècnica de Catalunya, Barcelona, Spain
[c] Dipartimento Politecnico di Ingegneria e Architettura, Università degli Studi di Udine, Unità di Ricerca INSTM Udine, Italy

ARTICLE INFO

Keywords:
Oxidation reaction
Heterogeneous catalysis
Ruthenium
Ceria-zirconia
Sustainable procedure

ABSTRACT

Selective oxidation of alcohols to aldehydes or ketones is a fundamental process in organic chemistry and the development of green and sustainable transformations are strongly required. Herein, we focused on the development of Ru-based catalysts deposited over ceria-zirconia supports (CZRu) for the solvent free oxidation of benzyl alcohol using air as oxidant, which is a cheap and safe process and meets to the atom economy and environment requirements. XPS characterization of the material reveals that the formation of RuO_2 on the surface is necessary to achieve higher catalytic activity. The activity is strongly related to the reducibility of the material and to the close interaction between ceria-zirconia and RuO_2, with the likely formation of Ru-O-Ce arrangements. The greater mobility of oxygen due to the formation of bridging oxygens in Ru-O-Ce and to the formation of superoxide species (O_2^-) over Ce^{3+} sites, significantly boosts the selective oxidation of alcohols. CZRu is a promising material with a remarkable 61% alcohol conversion at 90 °C without solvents; it also exhibits high activity (55% conversion) and complete selectivity (100%) for the selective oxidation of 1-phenylethanol to acetophenone. Overall, the formulation is among the most active reported so far under solvent free conditions and molecular oxygen. In addition, the reaction over CZRu exhibits an environmental factor (E-factor) lower than 1 (0.95) confirming the sustainability of the proposed process.

1. Introduction

Selective oxidation is among the most important reactions in industrial processes and in particular the oxidation of alcohols to carbonyl compounds is a fundamental step in synthetic organic chemistry due to the wide use of these products as precursors and/or intermediates of numerous compounds such as drugs, vitamins and fragrances [1–4]. Benzyl alcohol oxidation to benzaldehyde has been extensively studied due to the great importance of benzaldehyde as raw material for a large number of products [2,5,6]. In addition, benzyl alcohol oxidation is often use as a model reaction for the oxidation of alcohols [7]. Homogenous catalysts are widely investigated, but they show several drawbacks due to the difficult separation and recycling of the catalyst [8,9]. Recently, several studies on heterogeneous catalysts have been proposed [2,10-19]. Commonly, alcohol oxidations have been carried out in organic solvent in the presence of strong oxidants. Due to the strategical importance of these reactions, the enhancement of sustainable transformations is still a big challenge and great efforts are continually being made to develop aerobic oxidation methods that combine metal catalysts in solvent-free procedures (to reduce solvents), occurring in mild conditions (to save energy) and using molecular oxygen (cheap, safe and low-polluting oxidant) [12,20]. In the last thirty years [21,22], significant efforts have being made to develop greener processes and numerous green chemistry metrics have been identified to evaluate the sustainability of the reactions [23]. In this new vision, the chemical reaction is evaluated in a more global manner, taking into account several parameters such as the energy consumption, the origin of the reactants, the kind of solvent, the presence of toxic chemicals, the amount of waste, etc. [24]. Thus, the E-factor and the mass productivity [25,26] are suitable green chemistry parameters to compare different processes in terms of sustainability and environmental impact of our reaction.

* Corresponding author.
E-mail address: eleonora.aneggi@uniud.it (E. Aneggi).

https://doi.org/10.1016/j.mcat.2023.113049
Received 29 November 2022; Received in revised form 24 January 2023; Accepted 27 January 2023
Available online 7 March 2023

The E-factor (Eq. (1)) is focused on the quantity of waste that is produced for a given mass of product [23,27] and it had a main role in driving waste minimization and resource efficiency and developing waste-free processes. E-factor is an excellent metric of how green a reaction is, values closer to 0 indicates the goal of zero waste and more sustainable and greener process:

$$\mathrm{E-factor} = \frac{\text{mass waste}}{\text{mass of desired product}} \quad (1)$$

Mass productivity, MP (Eq. (2)) includes all the reactants, i.e. reagents, solvents, catalysts, and any other materials used in the reaction. It is the percentage of the ratio of the mass of the desired product to the total mass of the reactants. It is defined as the reciprocal converted to a percentage of the mass intensity (MI). The mass intensity and the E-factor are related each other through the eq. 3.

$$\mathrm{MP}(\%) = \frac{\text{mass of desired product} \times 100}{\text{total mass of used materials}} = \frac{1}{\mathrm{MI}} \times 100 \quad (2)$$

$$\mathrm{E-factor} = \mathrm{MI} - 1 \quad (3)$$

Ceria-based materials are widely used as a promoter or co-catalyst in several catalytic processes. The main application is in the automotive sector, where ceria is used in the three-way catalysts for the removal of CO, VOC and NOx from gasoline exhaust [28–31]. In addition, ceria, alone or in combination with transition/noble metals or other oxides, is exploited in several oxidation or hydrogenation reactions [32–34]. The key role of ceria in catalysis is mainly related to its oxygen storage capacity, the ability to reversibly remove/uptake oxygen from the fluorite lattice [35–37]. Redox properties of ceria could be strongly improved introducing other elements (such as Zr^{4+}) to form solid solution by replacing Ce^{4+}in the fluorite lattice [35,38]. Ceria-zirconia solid solutions exhibit higher thermal resistance and enhanced oxygen storage capacity and are widely used in several catalytic applications [35, 38-40]. Ceria alone has been also used in benzyl alcohol oxidation, although the activity is rather low [41]. To improve performances, the deposition of metal or metal oxide nanoparticles over ceria support is a promising strategy which takes advantage from the redox behavior and oxygen storage properties of ceria and the potential synergistic effects between the supported metal/metal oxide and the support. Ruthenium is a transition metal that has been effectively used in several oxidation reactions, both homogeneous and heterogeneous, for the treatment of organic substrates or inorganic pollutants [42–48]. The main purpose of this work is to immobilize Ru/RuO_x species over ceria and ceria-zirconia supports for the selective oxidation of benzyl alcohol carried out in a solvent free environment under air atmosphere. The main goal is to achieve a "greener" process; the measurement of environmental acceptability of the reaction with the new developed catalysts has been performed by two green chemistry metrics, the E-factor and the mass productivity. The idea is that the interfacial area between Ru/RuO_x particles and Ceria can act as a source of active oxygen thanks to the redox/oxygen storage behavior of ceria and to positive synergic interaction between Ce and Ru. The addition of zirconia can further enhance interaction by promoting oxygen exchange within the support.

2. Experimental

2.1. Catalyst preparation

A sample of commercial ceria (Treibacher AG) was used as received; ceria-zirconia solid solution of composition $Ce_{0.8}Zr_{0.2}O_2$ was prepared by co-precipitation of a solution of cerium and zirconium nitrate (Treibacher Industrie AG, Althofen, Austria) with NH_4OH (Sigma Aldrich) in the presence of H_2O_2. Briefly, 42.76 g of cerium nitrate and 12.85 g of zirconium nitrate are mixed together in presence of 32 mL of H_2O_2 (30% w/w in H_2O, Sigma Aldrich). The pH is progressively increased till 9.5 with ammonium hydroxide and the obtained suspension is mixed for 4 h. The formed precipitate is filtered, dried overnight at 100 °C and then calcined under static air at 500 °C for 3 h. Supported catalysts were prepared by incipient wetness (IW) using an aqueous solution of ruthenium nitrosyl nitrate (Sigma–Aldrich) in order to obtain Ru (2 wt %)/MxOy with MxOy = CeO_2 and $Ce_{0.8}Zr_{0.2}O_2$. Samples were then dried at 100 °C overnight and calcined at 500 °C for 3 h (CeRu and CZRu). All the materials were also treated at 300 °C for 2 h under 100 mL/min of 50%H_2/N_2 gas mixture (reduced samples are indicated as CeRu-R and CZRu-R).

2.2. Catalyst characterization

Textural characteristics were measured according to the B.E.T. method by nitrogen adsorption at 77 K, using a Tristar 3000 gas adsorption analyzer (Micromeritics). Structural features of the catalysts were investigated by X-ray diffraction. Diffraction patterns were recorded on a Philips X'Pert diffractometer (equipped with a real time multiple strip detector) operated at 40 kV and 40 mA using Ni-filtered Cu-Kα radiation. Diffraction patterns were collected using a step size of 0.02° and a counting time of 40 s per angular abscissa in the range 20°−145° The Philips X'Pert HighScore software was used for phase identification. The mean crystalline size was estimated from the full width at the half maximum (FWHM) of the X-ray diffraction peak using the Scherrer [49] equation with a correction for instrument line broadening. Rietveld refinement [50] of XRD patterns was performed by means of GSAS-EXPGUI program [51,52].

The reducibility of the catalysts was studied by temperature-programmed reduction (TPR) experiments (Autochem II 2920 Instrument, Micrometrics); catalysts (40 mg) without pretreatment were heated at a constant rate (10 °C/min) in a U-shaped quartz reactor from room temperature to 900 °C under a flowing hydrogen/nitrogen mixture (35 mL/min, 4.5% H_2 in N_2). The hydrogen consumption was monitored using a thermal conductivity detector (TCD). Quantification of H_2 consumption was carried out by calibrating the signal with the introduction of known amounts of hydrogen.

Raman spectra were collected with a Xplora Plus Micro-Raman system (Horiba, Kyoto, Japan) equipped with a cooled CCD detector (−60 °C) and Edge filter. The samples were excited with the 532 nm radiation. The spectral resolution was 1 cm^{-1} and the spectra acquisition was of 2 accumulations of 40 s with a 50× LWD objective. The optical images were collected with an integrated microscope Olympus BX43 (Olympus, Tokyo, Japan) with a 10× objective.

X-ray photoelectron spectroscopy (XPS) was performed on a SPECS system equipped with a XR50 source operating at 250 W and a Phoibos 150 MCD-9 detector. The energy step of high-resolution spectra was set at 0.05 eV. Atomic fractions were calculated using peak areas normalized on the basis of acquisition parameters after background subtraction, experimental sensitivity factors and transmission factors provided by the manufacturer. Cerium 3d spectra were deconvoluted using six peaks for Ce^{4+} (V, V'', V''', U, U'' and U''') and four peaks for Ce^{3+} (V_0, V', U_0 and U'), where U and V refer to the $3d_{3/2}$ and $3d_{5/2}$ spin-orbit components, respectively [53]. In-situ reduction treatments were carried out at 300 °C and 1 bar for 3 h under a H_2:Ar=1:1 mixture. The sample was heated with an IR lamp and the temperature was measured with a thermocouple in contact with the sample.

High resolution transmission electron microscopy (HRTEM) images were obtained by using a field emission gun FEI Tecnai F20 microscope equipped with a field emission source at an accelerating voltage of 200 kV, with a point-to-point resolution of 0.19 nm. The average particle diameter was calculated from the mean diameter frequency distribution with the formula: $d = \sum n_i d_i / \sum n_i$, where n_i is the number of particles with particle diameter d_i in a certain range.

2.3. Alcohol oxidation

Solvent-free oxidation of benzyl alcohol was carried out in a 5 mL round-bottom flask under reflux and continuous stirring conditions. For a typical run 0.2 g of catalyst, 1 mL of benzyl alcohol (9.7 mmol) and 0.01 g of hexamethylbenzene (Sigma Aldrich) as internal standard were placed in a flask and heated at the required temperature (70–90 °C) for 24 h under atmospheric pressure of O_2.

The progress of the reaction was checked by ^{1}H NMR using a Bruker Avance III HD 400 MHz spectrometer at 298 K equipped with carousel of 24 sample and automation program IconNMR which man-ages analysis from insertion of sample to integration of signal of spectra. The deuterated solvent, $CDCl_3$ (Sigma Aldrich) was used without any further purification. 10 μL of the reaction mixture was taken with a syringe and dissolved in 500 μL of anhydrous $CDCl_3$. The conversion was calculated from the integral area of the singlet at 4.72 ppm, corresponding to the -CH_2 protons of the benzyl alcohol, and compared with the hexamethylbenzene signals (2.30 ppm) as internal reference. Reported conversions are an average of three runs. The selectivity was evaluated through the analysis of the products obtained after reaction.

For the most promising catalyst, a free radical scavenger 2,6-di-tert-butyl-4-methylphenol (BHT) was added during the reaction to exclude the formation of radical intermediates.

Recycling of the catalyst has been investigated in multiple runs. After the first catalytic run, the catalyst was recovered by evaporation, dried under vacuum at 150 °C for 10 min and then reused in the next run under the same conditions. After each recovery, a loss of catalyst of about 2.5% was observed.

3. Results and discussion

3.1. Textural and structural characterization

Composition and textural/structural parameters of investigated materials are reported in Table 1. Ruthenium supported materials have a Ru content close to the nominal one, within the experimental error. All the materials show a surface area in the range 60–80 m^2/g. After impregnation of ceria and ceria-zirconia the surface area shows a slight decrease. The crystallite size obtained according to the Scherrer equation was about 6 nm for CZ-based materials and 12 nm for CeO_2-based catalysts. No differences in crystal size were observed after impregnation of ruthenium salt.

The structural characteristics of the catalysts were studied by XRD (Fig. 1).

For all the materials, peaks belonging to the support (CeO_2 or $Ce_{0.8}Zr_{0.2}O_2$) are clearly observed. The presence of very weak signals at $2\theta = 35.1°$and 54.5° suggests the formation of ruthenium oxide (RuO_2) in the samples after calcination. Although the XRD peaks are very low and close to the detection limit of the technique it is possible to obtain a preliminary information from this analysis. The results were then confirmed using XPS spectra. After treatment in H_2/N_2 the formation of metallic Ru was suggested by the disappearance of the RuO_2 peaks and the simultaneous evolution of a very low signal at $2\theta = 44°$ [54]. Rietveld analysis (Table 1) of investigated materials does not show any significant difference in the cell parameter after loading of Ru and after oxidation and reduction, thus indicating that Ru species are not entering in the fluorite structure of ceria or ceria-zirconia but remains very well dispersed over the surface.

For Ce-catalysts only a slight modification in cell parameter is observed due to a different amount of Ce^{3+} in the sample, as reported in Table 1.

CeRu and CZRu samples have been characterized by means of HRTEM analysis. Fig. 2A shows a representative image of the CeRu sample, which is constituted by crystalline ceria nanoparticles. The mean particle size of ceria is about 12±6 nm. The ceria nanoparticles are decorated by subnanometric entities, which show a darker electron contrast. A few of them are marked with arrows. Given the small dimensions of these entities, no lattice fringes can be observed, which prevents an exact identification of their nature. Nevertheless, the EDX spectrum recorded in the area shown in Fig. 2A reveals clearly the presence of Ru signal. This fact, together with the absence of any large Ru particle, suggests that the subnanometric entities correspond to a ruthenium phase. It is possible that Ru occurs as RuO_2 or as Ru-O-Ce assemblage. The EDX spectrum shows, in addition to Ru, the solely occurrence of Ce, O and Cu signals. Cu originates from the grid used for TEM measurements.

Fig. 2B shows a representative image of CZRu sample, which is constituted by crystalline ceria-zirconia nanoparticles. The mean particle size of the support crystallites is considerably lower than the previous sample, being about 5 ± 1 nm. Therefore, ceria-zirconia has a much narrower particle size distribution and shows a mean particle size lower than the ceria sample. In a similar way than the ceria sample, the ceria-zirconia nanoparticles are decorated by subnanometric entities, too (some of them marked with arrows). Again, given the small dimensions of these entities, no lattice fringes can be observed, which prevents an exact identification of their nature. Now, the EDX spectrum recorded in the area shown in Fig. 2B reveals, in addition to Ru, Ce and O (and Cu) signals, also the presence of Zr, as expected.

The particle size of ceria and ceria-zirconia crystallites are similar to the values calculated from the XRD patterns. HRTEM also allowed to identify the occurrence of ruthenium as subnanometric entities, very well dispersed on the supports, while, given the small dimensions of the entities, no lattice fringes were observed, preventing their exact identification as Ru or Ru oxide.

XPS analysis has been carried out to better elucidate the chemical state of Ruthenium (Table 2). Ru $3d_{5/2}$ peak has been used for the analysis of the chemical state of surface Ru. CeRu and CZRu showed one peak at binding energies of 280.7 and 281.0 eV, respectively, which were assigned to Ru^{4+} species, indicating that Ru over ceria-based materials is mainly in the oxidized state (RuO_2) [54].

After in situ-treatment under H_2 atmosphere, peaks attributed to RuO_2 disappeared and peaks at 280.2 eV due to metallic Ru species were

Table 1
Composition and textural characterization of investigated samples.

Sample	Surface area (m^2/g)	Crystallite size (nm)[a]	Cell parameter (Å)[b]	Molar composition[b]	Ru (wt.%)[c]
Ce	68	11.5	5.4141(2)	CeO_2 (0.70% Ce^{3+})	/
CeRu	62	11.5	5.4112(2)	CeO_2 (0.05% Ce^{3+})	1.89
CeRu-R	61	12.0	5.4125(2)	CeO_2 (0.35% Ce^{3+})	1.89
CZ	79	5.5	5.3653(4)	$Ce_{0.84}Zr_{0.16}O_2$	/
CZRu	72	5.5	5.3677(4)	$Ce_{0.85}Zr_{0.15}O_2$	1.98
CZRu-R	72	6.0	5.3681(2)	$Ce_{0.85}Zr_{0.15}O_2$	1.98

[a] calculated with Scherrer formula from X-ray diffraction patterns.
[b] from Rietveld refinement.
[c] from elemental analysis.

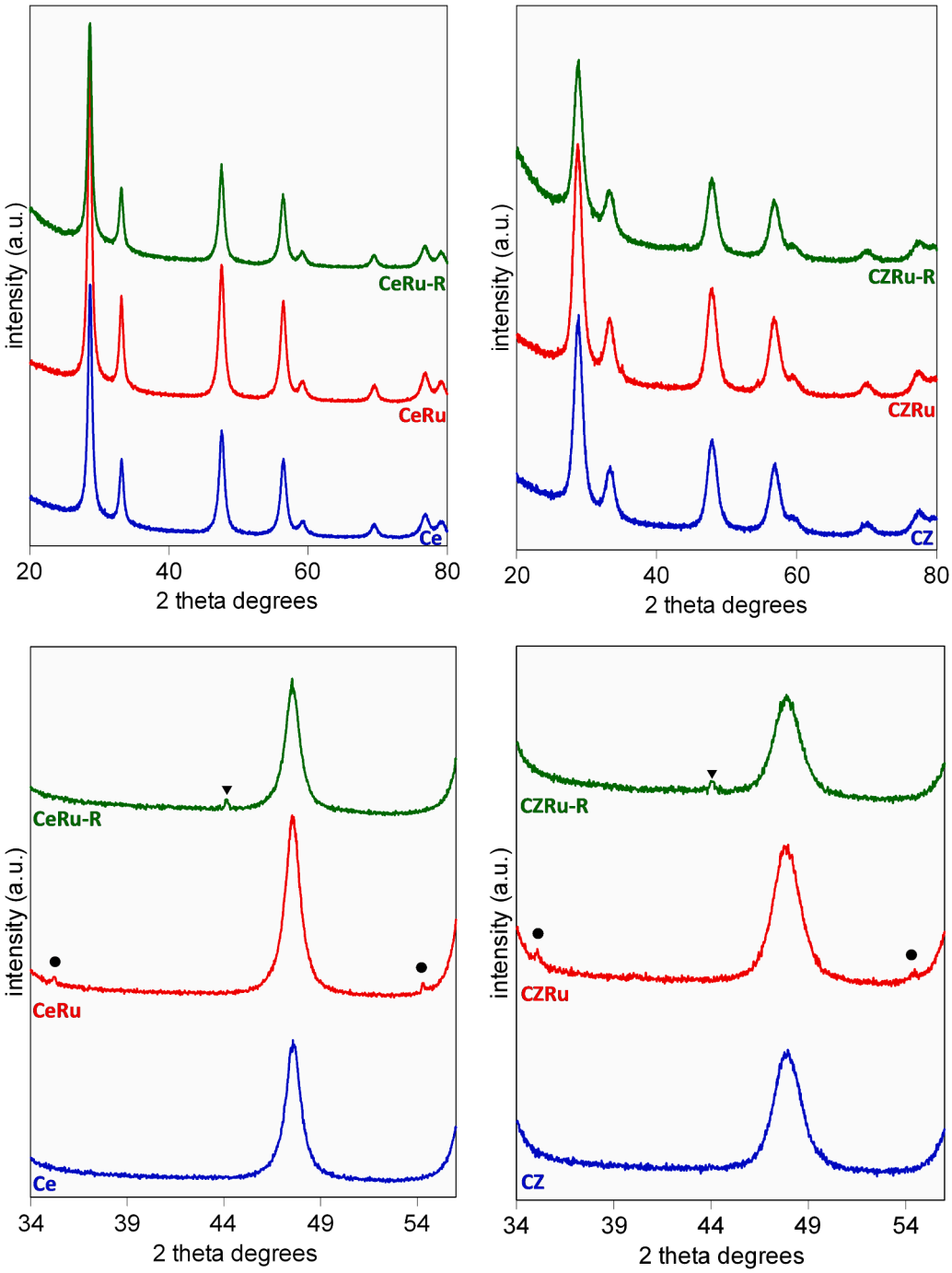

Fig. 1. XRD profiles of CeO_2 (left) and Ceria-zirconia (right) based catalysts. In the bottom, magnified zone of the range 34-56 2θ degrees are reported to highlight peaks belonging to Ru and RuO_2 (▼, Ru; • RuO_2).

identified. In both cases, the initial state of Ru is Ru oxide (most likely RuO_2), which evolves into metallic Ru after the in situ reduction treatment. Metallic Ru formed during the treatment is stable and does not completely oxidize back to RuO_2 due to exposure to ambient air. Metallic ruthenium is indeed visible in XRD profiles of reduced samples recorded under air atmosphere. HRTEM measurements have revealed that subnanometric ruthenium entities are very well dispersed on the supports, in perfect agreement with dispersion obtained by XPS analysis. Indeed, the Ru dispersion for the as prepared catalysts has been estimated from the signal ratio between Ru and Ce, Zr and it is almost double for CeRu compared to CZRu (0.154 versus 0.089, respectively); however, after in situ reduction the dispersion of CeRu decreases severely to 0.079, while it is rather stable to 0.083 for CZRu.

In addition, the atomic percentages of the elements present in the Ru-based catalysts obtained from elemental analysis were used to calculate bulk atomic ratios and for a comparison with atomic ratios obtained from XPS analysis (Table 2), which are representative of surface composition. The Ru/(Zr+Ce) atomic ratio is much higher from XPS than elemental analysis, highlighting the surface enrichment in Ru and a uniform dispersion of Ru particles on the surface. The analysis of O1s signals shows two peaks, one at 529.4–530.0 eV related to lattice oxygen (O_{latt}), the other at 531.6–532.9 eV assigned to surface oxygen (O_{surf}). The ratios of $O_{surf}/(O_{latt} + O_{surf})$ on CZRu is slightly higher than that on CeRu, revealing an higher content of surface oxygen over the ceria-

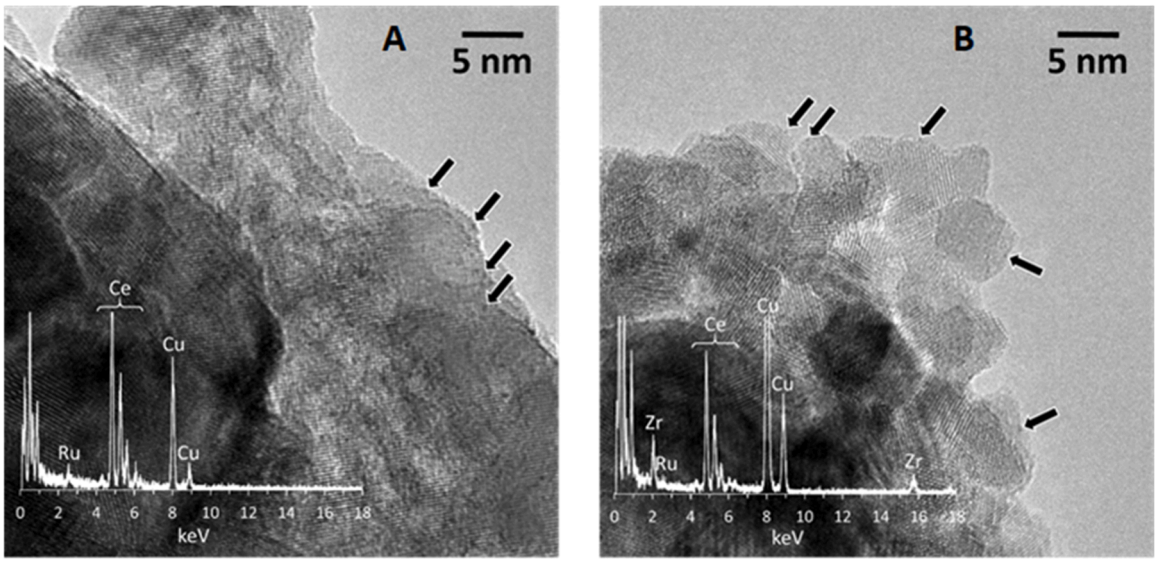

Fig. 2. HRTEM images for CeRu (A) and CZRu (B).

Table 2
XPS results of materials as prepared and after in situ reduction with H_2/Ar at 300 °C for 1 h and hydrogen consumption in H_2-TPR profiles in the region 50–200 °C.

Sample	Ru $3d_{5/2}$	Ce(III) %	$O_{(surf)}/(O_{surf}+O_{latt})$ % atomic	Ru/(Zr+Ce) % atomic[a]	Ru/(Zr+Ce) % atomic[b]	mmol H_2/g
CeRu	280.7 (RuO_2)	20.1	55.6	0.154	0.033	0.34
CeRu-R	280.2 (Ru)	28.2	60.0	0.079	0.033	/
CZRu	281.0 (RuO_2)	29.2	57.7	0.089	0.032	0.57
CZRu-R	280.2 (Ru)	31.1	63.6	0.083	0.032	0.68

[a] from XPS analysis.
[b] from elemental analysis.

zirconia sample, as shown in Fig. 3 (signals of the other elements have been reported in Figs. 1S and 2S). The increase of O_{surf} is usually related to the presence of surface adsorbed oxygen [55]. In addition, CZRu shows higher surface concentration of Ce^{3+} (29.2%) compared to CeRu (20.1%). As expected, after in situ reduction, the amount of surface oxygen and of Ce(III) increases for the two samples. In the case of small ceria crystallites (below 5 nm) Ce^{3+} sites are not necessarily related to oxygen vacancy and can easily adsorb oxygen producing active oxygen species and promoting oxygen storage capacity [56,57]. Previous investigations indicate that molecular oxygen can be easily activated by Ce^{3+} sites forming Ce^{4+}-O_2^- that is a very active and mobile species of surface oxygen [58,59]. As suggested by those studies, in CZRu the higher amount of Ce(III) significantly affects the creation of surface active oxygen species in the form of superoxide oxygen, O_2^-, enhancing oxidation activity already at low temperature due to the maximization of adsorption/release of active oxygen under operative conditions.

Reducibility of materials has also been investigated by H_2-TPR (Fig. 4). The reduction profile of pure CeO_2 is well known with the characteristic bimodal profile with two peaks at low and high temperature attributable, respectively, to the reduction of small crystallites and/or surface ceria and to the reduction of bulk and large ceria crystallites [60]. Ceria-zirconia sample displays a typical profile with one reduction peak around 500 °C [61], indicating a higher mobility of the oxygen species. The addition of Ru modifies the redox properties of CeO_2 and $Ce_{0.8}Zr_{0.2}O_2$ materials as a consequence of the Ru-CeO_2 interaction at the oxide interface and two distinguished sharp peaks are visible at low temperature (at around 80 °C and 120–130 °C).

These latter have been assigned to the reduction of RuO_2 with different strength of interaction with CeO_2-based support and surface Ce^{4+}. Indeed, bare RuO_2 shows only one peak at 170 °C, due to the direct reduction from Ru^{4+} to Ru^0 [62], while in our samples, the presence of more peaks suggests that Ru on CeO_2 exists in various states. Peak at lower temperature (around 80 °C) is related to the presence of very small ruthenium particles very well dispersed over the support, as evidenced by HRTEM images [63]. Hosokawa has studied in detailed the state of Ru on CeO_2 by coupling of several techniques, such as XRD, TPR, XANES and EXAFS spectra [64,65]. He found that the peak at lower temperature (around 70–80 °C) is related to the formation of bridging oxygens with ceria surface, Ru–O–Ce species, while the peak at higher temperature is due to Ru–O–Ru in the bulk RuO_2 oxide [63–66] as confirmed by XAFS analysis [67].

Considering the solid attribution of H_2-TPR peaks in ruthenium supported over ceria-based materials reported in literature, we can assume the presence of both Ru-O-Ce (low temperature peak, 80 °C) and Ru-O-Ru (high temperature peak, 120 °C) species . Ru-O-Ce bonds are unstable and the oxygen is very mobile and it is easily reduced at very low temperature. In addition, the reduction signal of ceria and ceria-zirconia at around 500 °C is shifted at lower temperature, indicating that Ru-species promotes surface ceria reduction at a much lower temperature. For CeRu-R a very low signal at around 150 °C is still visible, while CZRu-R shows in the low temperature region a very sharp peak. In Table 2 a quantitative analysis of TPR profiles in the region 50–200 °C is reported.

For CZRu and CZRu-R the quantitative analysis of the TPR profile reveals that a part of Ce^{4+} is reduced between 50 and 200 °C; the amount of hydrogen consumption in this temperature range (respectively 0.57 and 0.68 mmol/g_{cat}) is larger than that required for the complete reduction of RuO_2 (0.39 mmol/g_{cat}), while CeRu shows a hydrogen consumption comparable with the theoretical amount. TPR results suggest that reduction of $Ce_{0.8}Zr_{0.2}O_2$ is significantly enhanced by the

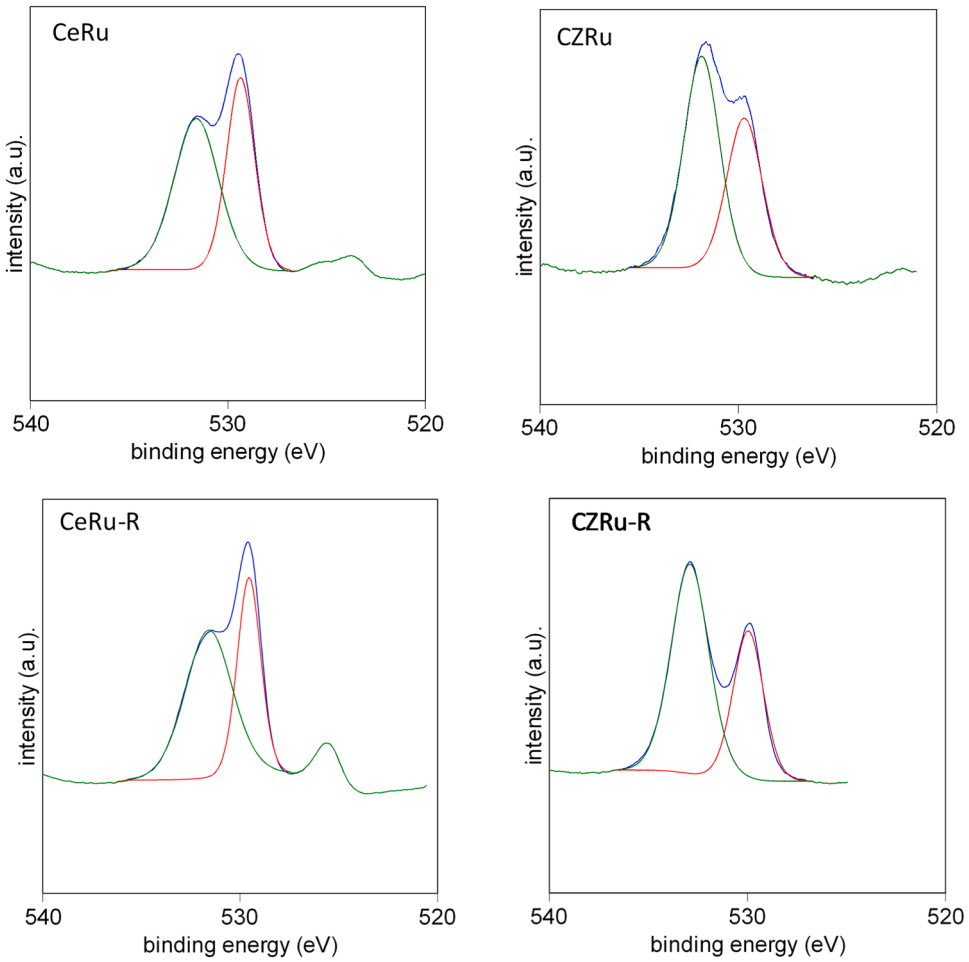

Fig. 3. XPS spectra of O 1s photoelectrons for CeO_2 (left) and Ceria-zirconia (right) based catalysts (O_{latt} in red and O_{surf} in green).

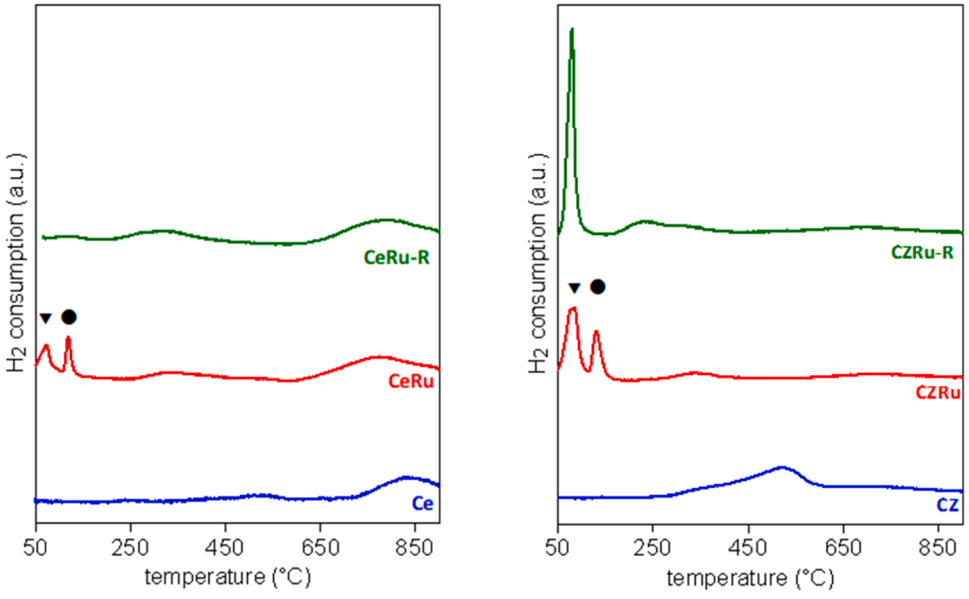

Fig. 4. TPR profiles of investigated samples (▼ peak at around 80 °C due to Ru-O-Ce; • peak at around 120 °C due to Ru-O-Ru).

Ru species dispersed over the surface and takes place simultaneously with RuO_2 reduction at very low temperature (50–200 °C). The enhancement of $Ce_{0.8}Zr_{0.2}O_2$ reduction can be due to hydrogen spillover from Ru to ceria or to the transfer of oxygen from $Ce_{0.8}Zr_{0.2}O_2$ to Ru with formation of more reducible oxygen species [54,68]. It is worth noting the high consumption of hydrogen which is observed for CZ2Ru-R; in this sample Ru species are in metallic state as revealed by XRD and XPS analysis and consequently, the hydrogen consumption is only due to

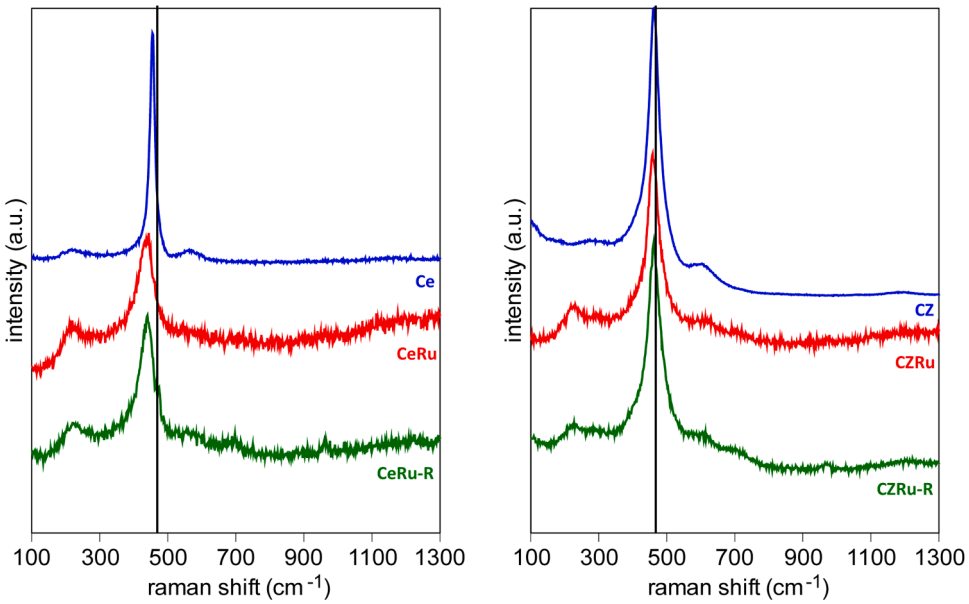

Fig. 5. Raman profiles for Ce and CZ-based catalysts (black line indicates 465 cm^{-1}).

Table 3
FWHM and peak intensity ratio (I_D/I_{F2g}) from Raman spectra.

sample	FWHM (cm^{-1})	I_D/I_{F2g}
Ce	22	0.06
CeRu	50	0.08
CeRu-R	48	0.09
CZ	35	0.05
CZRu	50	0.09
CZRu-R	46	0.10

CeO_2 reduction, indicating that Ru^0 over CZ induces higher reducibility of the support compared to RuO_2. These findings are in good agreement with previous studies on Ru over ceria-based catalysts [54,64].

The catalysts were also characterized using laser Raman spectroscopy (Fig. 5).

Commonly, cerium oxide has Raman active triply degenerate F_{2g} mode at 465 cm^{-1} (black line in the Fig. 5) which is characteristic of the cubic fluorite phase. The investigated CeO_2 samples show one Raman mode, centered at 455 cm^{-1}; the stronger red shift to 455 cm^{-1} of our samples is mainly due to the small dimension of the crystallites [69–71].

Generally, the introduction of Zr in CeO_2 fluorite structure leads to a blue-shift (from 465 to 473 cm^{-1}) due to substitution of $Ce^{4+}$by smaller Zr^{4+} cations, indeed, Raman mode shifts upwards as the cell parameter decreases and vice-versa [71]. In our samples a blue-shift from 455 to 460 cm^{-1} is observed due to the small crystallite size of our materials. When Ru is added to the supports, a broadening in the full width at half maximum (FWHM) values of F_{2g} peaks is observed (Table 3) that is correlated to high concentration of defects in the sample due to the strong interaction between ruthenium species and Ce-based materials with formation of Ru-O-Ce [72,73].

Besides the main band, the Raman spectrum of CeO_2/CZ materials shows additional peaks at around 220 (due to second-order transverse acoustic, 2TA mode) and 570 cm^{-1} (defect-induced, D mode), that generally are attributed to oxygen defects in the fluorite structure [69, 70,74,75].

A detailed analysis of the Raman profiles, provides interesting findings on the formation of oxygen defects due to the presence of Ru species. Characteristic bands of RuO_2 at 528, 644 and 716 cm^{-1} are not visible in the Raman profile probably because they are too weak compared to CeO_2 bands [76].

In the Ru-based catalysts, the ratio of the Raman peak at 560 cm^{-1} to the peak at 455 cm^{-1} (I_D/I_{F2g}) increases (Table 3), suggesting an increase in the oxygen defect concentration for ceria-based catalysts [71, 74,77]. After addition of ruthenium, the samples show two new peaks at around 700 and 970–980 cm^{-1}, that are better defined after reduction. These peaks are assigned to Ru-O-Ce bond [72,73]. The increase in oxygen vacancies in Ru-doped ceria and CZ catalysts, will lead to more active oxygen species on the surface of the catalysts, and this will be an important descriptor for catalyst activity. Summarizing, the addition of ruthenium to ceria-zirconia supports significantly promote the formation of surface active oxygen specie, O* (Scheme 1) such as bridging oxygens (Ru-O-Ce) and superoxide species (O_2^-), as evidenced by XPS, H_2-TPR and Raman analysis.

3.2. Catalytic activity

Benzyl alcohol oxidation to benzaldehyde has been carried out under air at 70 or 90 °C for 24 h. ^{1}H NMR spectroscopy has been used for the quantitative analysis of the conversion and selectivity of benzyl alcohol oxidation to benzaldehyde. The ^{1}H NMR spectrum of benzyl alcohol shows a multiplet at 7.43–7.29 ppm bearing to the protons of the aromatic ring, and a singlet at 4.72 ppm corresponding to the methylene group. The formation of the benzaldehyde gives rise to new sets of signals. Specifically, the signal at about 10 ppm is attributed to the proton resonance of the aldehyde group and from 7.87 to 7.51 ppm the signals are related to the phenyl group. A detailed analysis of the ^{1}H NMR spectrum does not reveal formation of any other reaction products arising from further oxidation, indicating that the reaction is completely selective.

Preliminary tests over bare supports evidenced no conversion in the oxidation of benzyl alcohol in this temperature range and therefore, exclude any oxidation activity of the oxides under these conditions; these results also exclude important adsorption effects of the substrate on the catalyst surface. At 70 °C, CeRu and CZRu are moderately active with a conversion in the range 18–38%, while an increase in the reaction temperature (90 °C), resulted in an improvement of conversion, respectively to 29 and 61%. The selectivity to benzaldehyde was always complete (Fig. 6).

CZRu results to be significantly active also for secondary alcohol (1-phenylethanol) oxidation with a conversion of around 55% and a complete selectivity to acetophenone (red bar in Fig. 6).

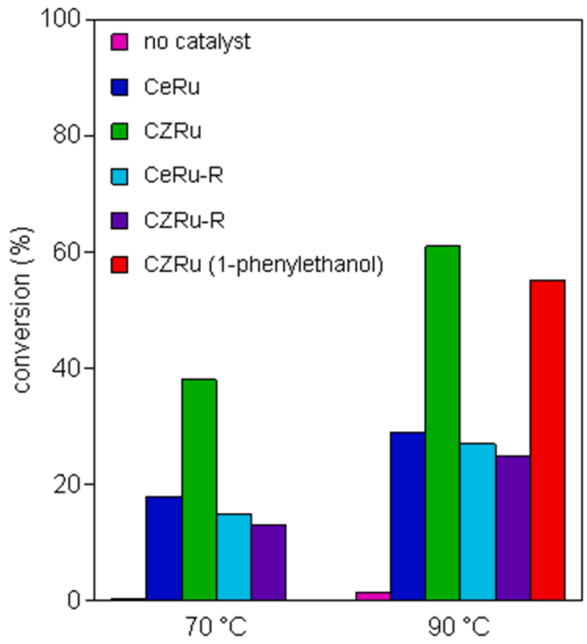

Fig. 6. Selective conversion of benzyl alcohol to benzaldehyde. Red bar shows oxidation of a 1-phenylethanol to acetophenone (reaction conditions: 1 mL of benzyl alcohol (or 1-phenylethanol) 200 mg of catalyst, 90 °C for 24 h, 10 mg of hexamethylbenzene as internal standard).

CZRu is the most active material with a remarkable conversion of 61% at 90 °C, resulting among the most active heterogeneous catalyst reported in literature under solvent free conditions (Table 4).

A direct comparison between the different reactions is rather difficult due to the extreme variation of the reaction parameters and in particular the amount of O_2 used.

Pd supported on different metal oxides (Pd/SiO_2-Al_2O_3 and Au-Pd/CeO_2 rod) are particularly active (93–97% of conversion), but the reactions were carried out either under 3 atm of pure O_2 or in O_2 flow (3 mL / min) thus favoring the reaction [78,80]. Non-supported colloidal Ru nanoparticles [79] result to be a very effective catalyst for oxidation of benzyl alcohol to benzaldehyde with a conversion of 93% and a selectivity of 90%, but the reaction has been carried out at severe conditions, under 10 atm of pure O_2 in an autoclave. A comparison of reactions carried out at atmospheric pressure evidenced that Ru-supported on ceria-based materials are promising formulations (Ru/CeO_2 reached a conversion of 67% and a selectivity of 91% [68] while Ru/CZ [this study] achieved 61% of conversion and complete selectivity).

For a better understanding of the process sustainability, we have considered two green chemistry metrics, the E-factor and the MP (mass productivity) and results for the catalytic reactions carried out under atmospheric pressure are reported in Fig. 7. Ru/CZ achieved the best results in green chemistry metrics, with a e-factor lower than 1 (0.95) and a MP of 51% demonstrating to be an ideal material with low environmental impact for the oxidation of benzyl alcohol in terms not only of conversion and selectivity but also of sustainability of the process and reduction of waste. A E-factor of 0.95 is typical of bulk chemistry sector [25].

The conversion of benzyl alcohol shows a dependence on the reaction temperature, with better activity at higher temperature. This increase is not only due to kinetic effect on the catalytic reaction, but is mainly related to the favored reduction of RuO_2 at the higher temperature (see H_2-TPR profiles). This can also explain the higher increase in activity observed for CZRu, in agreement with the intensity of the H_2-TPR peak at 80 °C.

Benzyl alcohol oxidation has been also carried out over reduced materials at 90 °C; CeRu-R does not change its activity (27% conversion), while CZRu-R show a severe decrease of conversion from 61 to 25%. It seems likely that when ruthenium is in a metallic state, the activity can reach a maximum at around 25–27% conversion independent from the support, while when RuO_2 is formed on the surface the activity is higher and is mainly related to the reducibility of the catalyst. CZRu exhibits the higher activity (around 61%) and is characterized by higher hydrogen consumption during reduction (0.57 mmol H_2/g), while CeRu shows a lower hydrogen consumption 0.34 mmol H_2/g and about half conversion in the same conditions (29%).

The remarkable activity of our Ru/CZ catalyst has been also confirmed carrying out the reaction in the presence of a solvent where conversion of 90% and 100% selectivity was found (Fig. 3S), indeed, for solvent-based reactions, Ru-based materials reported in literature show very different conversion results ranging from 13% to 100% [87–89].

To exclude the possibility of a radical chain process, for CZRu the reaction has been carried out in the presence of a radical scavenger (2,6-Di-tert-butyl-4-methylphenol) and does not show any difference in conversion indicating that active free radicals are not generated.

In addition, the reusability of the most promising catalyst, CZRu, at

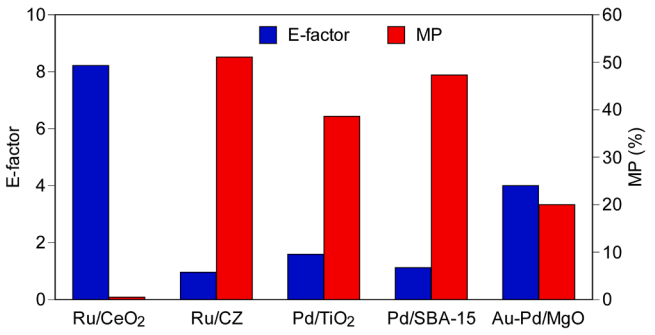

Fig. 7. Comparison of E-factor and mass productivity (MP) for benzyl alcohol oxidation over heterogeneous catalyst.

Table 4
Comparison of results for benzyl alcohol oxidation over heterogeneous catalyst in solvent free reaction.

catalyst	Catalyst (mg)	Alcohol (mmol)	O_2	T (°C)	Time (h)	Conv (%)	Select (%)	Ref
Pd/SiO_2-Al_2O_3	100	48.5	3 mL/min	70	10	97	98	[78]
Ru	20	27.7	10 atm	100	5	93	90	[79]
Au-Pd/CeO_2 rod	50	144	3 atm	120	3	78	88	[80]
Ru/CeO_2	500	1[a]	1 atm	50	4	67	91	[68]
Ru/CZ	200	9.6	1 atm	90	24	61	100	this study
Au/CeO_2	150	48	5 atm	150	24	52	93	[81]
Pd/TiO_2	20	18	1 atm	120	1	52	75	[82]
Pd/SBA-15	50	96	1 atm	95	3.5	50	95	[83]
Pd/TiO_2	100	96	90 mL/min	90	2	39.5	72.9	[84]
Au-Pd/MgO	200	18	1 atm	120	4	20	97	[85]
Au/TiO_2	200	96	2 atm	100	5	2.5	100	[86]

[a] 1 mmol of alcohol in 5 mL of acetonitrile. Reaction carried out in solvent, 10 mL of acetonitrile.

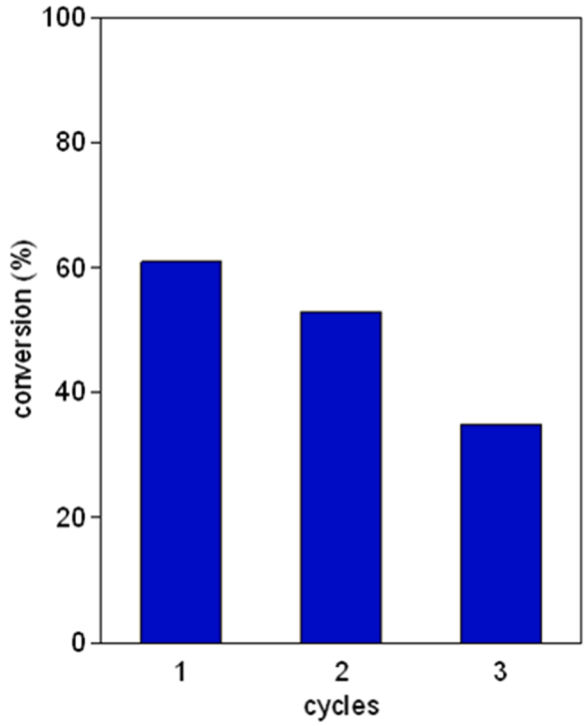

Fig. 8. Reusability of CZRu (selectivity is 100%). Reaction conditions: 1 mL of benzyl alcohol, 200 mg of catalyst, 90 °C for 24 h, 10 mg of hexamethylbenzene as internal standard.

90 °C over two further reaction cycles was investigated. After the first run, the used catalyst was recovered by evaporation and then it has been reused under the same conditions. The results reported in Fig. 8 indicate that, while the selectivity to benzaldehyde does not change the conversion decreases to 35% in the third cycle.

XPS analysis of the CZRu sample after used has been carried out (Fig. 4S). Ru $3d_{5/2}$ peak has been used for the analysis of the chemical state of surface Ru and the material show one peak at binding energies of 281.0 eV that were assigned to Ru^{4+} species, indicating that, after used,

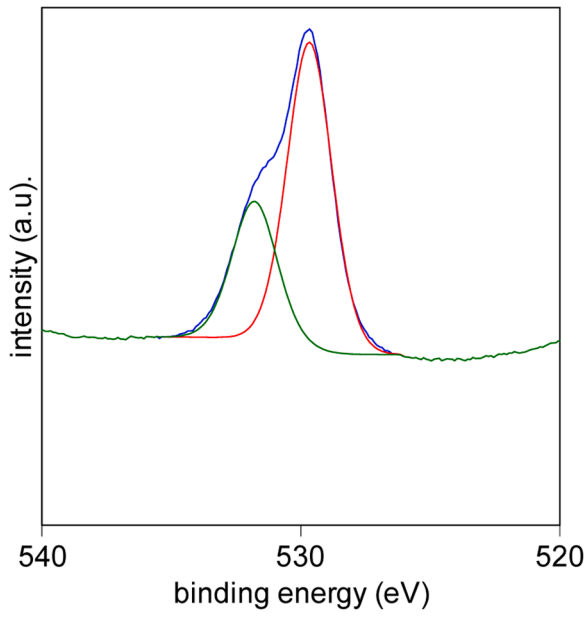

Fig. 9. XPS spectra of O 1s photoelectrons for CZRu after use (O_{latt} in red and O_{surf} in green).

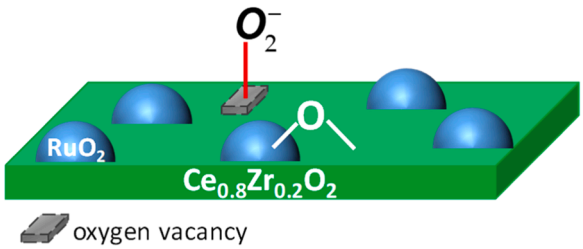

Scheme 1. Surface active oxygens species (O*) on Ru/CZ.

Ru over ceria-based materials is again mainly in the oxidized state (RuO_2). The dispersion of Ru after used, estimated from the signal ratio between Ru and Ce, Zr, is rather stable with respect to the fresh catalyst (0.092 versus 0.089, respectively).

The analysis of O1s signals shows two peaks, one at 529.4–530.0 eV related to lattice oxygen (O_{latt}), the other at 531.6–532.9 eV assigned to surface oxygen (O_{surf}). The ratios of $O_{surf}/(O_{latt} + O_{surf})$ on CZRu after used significantly decreases, revealing a lower content of surface oxygen after the reaction, as shown in Fig. 9. In addition, the used CZRu shows a lower surface concentration of Ce^{3+} (24.1%) than the fresh catalyst (29.2%). The decrease of $O_{surf}/(O_{latt} + O_{surf})$ ratio and of the amount of Ce(III) after reaction, is in agreement with the decrease of the conversion. Indeed, the lower amount of Ce(III) can affect the formation of surface active oxygen species in the form of superoxide oxygen, O_2^-, invalidating the oxidation activity.

The possibility of reuse of the catalyst affects the sustainability of the process. A comparison was made between the CZRu system developed in this study and the Au-Pd / MgO catalyst prepared by Alshammari et al. [85]. In both cases the material was reused three times. The conversion at the third cycle is reduced by about 40% for CZRu and by 77% for Au-Pd / MgO. The E-factor slightly increases for CZRu from 0.95 to 1.86 while the effect of recycles for Au-Pd / MgO is significant with an increase from 8 to 39. At the third recycle CZRu has a mass productivity of 35%, while the value drops to 2.5 for Au-Pd / MgO. This further analysis of green chemistry metrics confirms the promising activity of the developed CZRu catalyst.

Summarizing, the catalytic activity is related, from one side, to the state of Ru over the supports, with ruthenium oxide more active compared to metallic Ru, and from the other side, to the reducibility and oxygen mobility of the materials. XPS, H_2-TPR and XRD measurements show the formation of RuO_2 on CeRu and CZRu, while metallic ruthenium prevails on reduced samples (CeRu-R and CZRu-R). Catalytic tests evidenced the higher activity of CeRu and CZRu compared to reduced materials CeRu-R and CZRu-R, suggesting a key role of RuO_2 in the selective oxidation reaction. Indeed, Ru-species promote surface ceria reduction at low temperature, in the range 80–130 °C, and this specific reduction behavior of RuO_2 on Ce and CZ plays a crucial role in the enhancement of the catalytic activity for the selective oxidation of benzyl alcohol.

The activity could be probably related to the increased mobility of surface oxygen induced by the presence of RuO_2 species and the formation of Ru–O–Ce and superoxide O_2^- over Ce^{3+} sites; this effect is much higher for CZ compared to Ce, due to the promotion induced by zirconia substitution [90]. The strong metal-support interaction between RuO_2 and CZ boosts the oxidation capacity of the catalyst [90]. Indeed, the amount of Ce^{3+}that is strictly related to the formation of surface active oxygen species, as reveled by XPS analysis, is higher for CZRu compared to CeRu (29% vs 20%) significantly enhancing the oxidation capacity at low temperature. By contrast, the dispersion of ruthenium species on the surface does not play a significant role in the reaction.

In light of these findings, it can be assumed that the activity is strongly related to the reducibility of the material and to the close interaction between ceria-zirconia and RuO_2 with the formation of

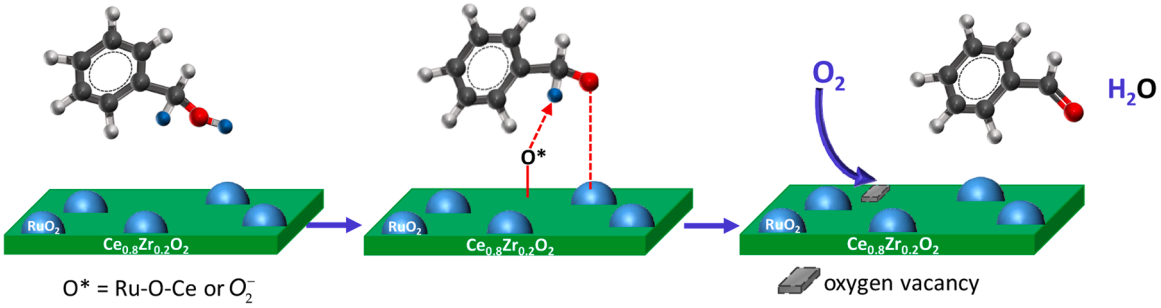

Scheme 2. Possible mechanism of oxidation of benzyl alcohol over CZRu catalyst.

bridging oxygen Ru-O-Ce and superoxide species. This metal-support interaction leads to a greater mobility of oxygen at low temperatures and the coupling of the $Ce^{4+}/Ce^{3+}$and Ru^{4+}/Ru redox cycles considerably increases the catalytic activity. These findings are in good agreement with previous results on Ru over ceria-based catalysts in different catalytic reactions [64,90,91].

Conceivable reaction path can be proposed where active oxygen species (bridging oxygen Ru-O-Ce and Ce^{4+}-O_2^-), which are very mobile and reducible at low temperature, play a fundamental role likely through a Mars-van Krevelen mechanism (Scheme 2) [79]. The first step is the adsorption and deprotonation of alcohol over CZRu with formation of the alkoxide intermediate and activation of C—H bond in β position [12], followed by the desorption of benzaldehyde and water. Then, the vacancy formed on CZ surface during the reaction is filled by molecular oxygen.

4. Conclusion

We have shown that ruthenium supported over ceria-zirconia is a promising material for the selective oxidation of benzyl alcohol to benzaldehyde, with a remarkable conversion of 61% at 90 °C, resulting among the most active catalyst reported in the literature. The reaction is carried out in the presence of molecular oxygen and under solvent free conditions following a "green procedure" in the light of a better environmental sustainability. The E-factor lower than 1 and a mass productivity of 51% confirmed the sustainability of the process.

The activity of the catalyst is not related to the dispersion of ruthenium species over the support, but is strongly affected by the reducibility of the material and to the close interaction between ceria-zirconia and RuO_2. The formation of active oxygen species such as superoxide and bridging oxygen between ceria and ruthenium (Ru-O-Ce), is responsible for the enhancement of the oxygen mobility and the reducibility at very low temperature which then promote a significant conversion and a complete selectivity in the oxidation reaction.

The work reported here is a preliminary study paving the way for future research on heterogeneous catalysts for the oxidation of organic molecules for the production of fine chemicals in more sustainable reaction conditions without the use of solvents, compared to traditional reactions. The practical impact of our study is the assessment of a new green approach for the catalytic oxidation of alcohols. Indeed, it is important to change the traditional synthesis route into greener and more sustainable reactions. In the future we plan to investigate the oxidation of other molecules and to evaluate the possibility of suitably modifying the formulations to improve their reusability.

Declaration of Competing Interest

The authors declare that they have no known competing financial interests or personal relationships that could have appeared to influence the work reported in this paper

Acknowledgements

JL is a Serra Húnter Fellow and is grateful to ICREA Academia program and projects MICINN/FEDER PID2021-124572OB-C31 and GC 2021 SGR 01061.

"This contribution is dedicated to Prof. Rosario Pietropaolo, a visionary of science, master of ethics and dedication and inspiration for many of us."

CRediT authorship contribution statement

Conceptualization, E.A., D.Z.; Methodology, E.A., D.Z.; Investigation, E.A., J.L, J.S., F.C.; Data Curation, E.A.; Funding Acquisition, A.T., Resources, W.B., A.T., D.Z.; Writing—Original Draft Preparation, E.A.; Writing—Review and Editing, E.A., W.B., J.L., A.T., D.Z.

Supplementary materials

Supplementary material associated with this article can be found, in the online version, at doi:10.1016/j.mcat.2023.113049.

References

[1] R. Sheldon, J. Kochi, Activation of Molecular Oxygen By Metal complexes. Metal-Catalyzed Oxidations of Organic Compounds, Academic Press, New York, 1981.
[2] T. Mallat, A. Baiker, Oxidation of alcohols with molecular oxygen on solid catalysts, Chem. Rev. 104 (2004) 3037–3058, https://doi.org/10.1021/cr0200116.
[3] H. Goksu, F. Sen, Handy and highly efficient oxidation of benzylic alcohols to the benzaldehyde derivatives using heterogeneous Pd/AlO(OH) nanoparticles in solvent-free conditions, Sci Rep-Uk 10 (2020) 5731, https://doi.org/10.1038/S41598-020-62695-4.
[4] M.N. Kopylovich, A.P.C. Ribeiro, E.C.B.A. Alegria, N.M.R. Martins, L.M.D.R. S. Martins, A.J.L. Pombeiro, Chapter three - catalytic oxidation of alcohols: recent advances, in: P.J. Pérez (Ed.), Advances in Organometallic Chemistry, Academic Press, 2015, pp. 91–174.
[5] R.A. Sheldon, I.W.C.E. Arends, G.-.J. ten Brink, A. Dijksman, Green, catalytic oxidations of alcohols, Account. Chem. Res. 35 (2002) 774–781, https://doi.org/10.1021/ar010075n.
[6] S. Xu, J. Wu, P. Huang, C. Lao, H. Lai, Y. Wang, Z. Wang, G. Zhong, X. Fu, F. Peng, Selective catalytic oxidation of benzyl alcohol to benzaldehyde by nitrates, Front. Chem. 8 (2020) 151, https://doi.org/10.3389/fchem.2020.00151.
[7] C.M. Crombie, R.J. Lewis, R.L. Taylor, D.J. Morgan, T.E. Davies, A. Folli, D. M. Murphy, J.K. Edwards, J. Qi, H. Jiang, C.J. Kiely, X. Liu, M.S. Skjøth-Rasmussen, G.J. Hutchings, Enhanced selective oxidation of benzyl alcohol via in situ H2O2 production over supported Pd-based catalysts, Acs Catal. 11 (2021) 2701–2714, https://doi.org/10.1021/acscatal.0c04586.
[8] M.J. Schultz, M.S. Sigman, Recent advances in homogeneous transition metal-catalyzed aerobic alcohol oxidations, Tetrahedron 62 (2006) 8227–8241, https://doi.org/10.1016/j.tet.2006.06.065.
[9] C.E. Chan-Thaw, A. Savara, A. Villa, Selective benzyl alcohol oxidation over Pd catalysts, Catalysts 8 (2018) 431. ttps://doi.org/10.3390/catal8100431.
[10] C.P. Vinod, K. Wilson, A.F. Lee, Recent advances in the heterogeneously catalysed aerobic selective oxidation of alcohols, J. Chem. Technol. Biot. 86 (2011) 161–171, https://doi.org/10.1002/jctb.2504.
[11] S.E. Davis, M.S. Ide, R.J. Davis, Selective oxidation of alcohols and aldehydes over supported metal nanoparticles, Green Chem. 15 (2013) 17–45, https://doi.org/10.1039/c2gc36441g.
[12] C. Xu, C. Zhang, H. Li, X. Zhao, L. Song, X. Li, An overview of selective oxidation of alcohols: catalysts, oxidants and reaction mechanisms, Catal. Surv. Asia 20 (2015) 13–22, https://doi.org/10.1007/s10563-015-9199-x.

[13] A.S. Sharma, H. Kaur, D. Shah, Selective oxidation of alcohols by supported gold nanoparticles: recent advances, RSC Adv. 6 (2016) 28688–28727, https://doi.org/10.1039/c5ra25646a.

[14] C.E. Chan-Thaw, A. Savara, A. Villa, Selective benzyl alcohol oxidation over Pd catalysts, Catalysts 8 (2018) 431, https://doi.org/10.3390/Catal8100431.

[15] B. Das, M. Sharma, M.J. Baruah, B.P. Mounash, G.V. Karunakar, K.K. Bania, Gold nanoparticle supported on mesoporous vanadium oxide for photo-oxidation of 2-naphthol with hydrogen peroxide and aerobic oxidation of benzyl alcohols, J. Environ. Chem. Eng. 8 (2020), 104268, https://doi.org/10.1016/j.jece.2020.104268.

[16] C. Cui, X. Zhao, X. Su, W. Gao, J. Zhan, X. Zhang, G. Li, X.L. Zhang, Y. Sang, H. Liu, Selective oxidation of benzyl alcohol using a Ni(OH)2-modified CdS-MoS2 composite photocatalyst under ambient conditions, J. Environ. Chem. Eng. 9 (2021), 106416, https://doi.org/10.1016/j.jece.2021.106416.

[17] M. Bellardita, S. Yurdakal, B.S. Tek, Ç. Değirmenci, G. Palmisano, V. Loddo, L. Palmisano, J. Soria, J. Sanz, V. Augugliaro, Tuning the selectivity to aldehyde via pH regulation in the photocatalytic oxidation of 4-methoxybenzyl alcohol and vanillyl alcohol by TiO2 catalysts, J. Environ. Chem. Eng. 9 (2021), 105308, https://doi.org/10.1016/j.jece.2021.105308.

[18] D. Sarkar, K.S. Paliwal, S. Ganguli, A.E. Praveen, D. Saha, V. Mahalingam, Engineering of oxygen vacancy as defect sites in silicates for removal of diverse organic pollutants and enhanced aromatic alcohol oxidation, J. Environ. Chem. Eng. 9 (2021), 105134, https://doi.org/10.1016/j.jece.2021.105134.

[19] Y. Fan, Y. Mo, X. Zhao, X. Zuo, J. Nan, X. Xiao, In-situ construction of Bi24O31Br10-decorated self-supported BiOBr microspheres for efficient and selective photocatalytic oxidation of aromatic alcohols to aldehydes under blue LED irradiation, J. Environ. Chem. Eng. 10 (2022), 107382, https://doi.org/10.1016/j.jece.2022.107382.

[20] S. Lukato, O.F. Wendt, R. Wallenberg, G.N. Kasozi, B. Naziriwo, A. Persson, L. C. Folkers, E. Tebandeke, Selective oxidation of benzyl alcohols with molecular oxygen as the oxidant using Ag-Cu catalysts supported on polyoxometalates, Result. Chem. 3 (2021), 100150, https://doi.org/10.1016/j.rechem.2021.100150.

[21] P.T. Anastas, D.T. Allen, Twenty-five years of green chemistry and green engineering: the end of the beginning, ACS Sustain. Chem. Eng. 4 (2016), https://doi.org/10.1021/acssuschemeng.6b02484, 5820-5820.

[22] P. Anastas, B. Han, W. Leitner, M. Poliakoff, Happy silver anniversary": green Chemistry at 25, Green Chem. 18 (2016) 12–13, https://doi.org/10.1039/c5gc90067k.

[23] C.J. Clarke, W.-.C. Tu, O. Levers, A. Bröhl, J.P. Hallett, Green and sustainable solvents in chemical processes, Chem. Rev. 118 (2018) 747–800, https://doi.org/10.1021/acs.chemrev.7b00571.

[24] D.J.C. Constable, A.D. Curzons, V.L. Cunningham, Metrics to 'green' chemistry—which are the best? Green Chem. 4 (2002) 521–527, https://doi.org/10.1039/b206169b.

[25] R.A. Sheldon, The E factor 25 years on: the rise of green chemistry and sustainability, Green Chem. 19 (2017) 18–43, https://doi.org/10.1039/c6gc02157c.

[26] R.A. Sheldon, Metrics of green chemistry and sustainability: past, present, and future, ACS Sustain. Chem. Eng. 6 (2018) 32–48, https://doi.org/10.1021/acssuschemeng.7b03505.

[27] A.R. Sheldon, Organic synthesis. Past, present and future, Chem. Ind.-Lond. 23 (1992) 3.

[28] J. Kaspar, P. Fornasiero, M. Graziani, Use of CeO2-based oxides in the three-way catalysis, Catal. Today 50 (1999) 285–298, https://doi.org/10.1016/S0920-5861(98)00510-0.

[29] A. Trovarelli, Paolo Fornasiero, Catalysis By Ceria and Related Materials, Imperial College Press, London (UK), 2013, 2nd Edition.

[30] E. Aneggi, M. Boaro, S. Colussi, C. de Leitenburg, A. Trovarelli, Ceria-based materials in catalysis: historical perspective and future trends, Handb. Phys. Chem. Rare Earth. 50 (2016) 209–242, https://doi.org/10.1016/bs.hpcre.2016.05.002.

[31] E. Aneggi, C. de Leitenburg, M. Boaro, P. Fornasiero, A. Trovarelli, Catalytic Applications of Cerium dioxide, Cerium Oxide (CeO_2): Synthesis, Properties and Applications, Elsevier, 2020, pp. 45-108.

[32] R.J. Gorte, Ceria in catalysis: from automotive applications to the water-gas shift reaction, Aiche J. 56 (2010), https://doi.org/10.1002/aic.12234. NA-NA.

[33] T. Montini, M. Melchionna, M. Monai, P. Fornasiero, Fundamentals and catalytic applications of CeO2-based materials, Chem. Rev. 116 (2016) 5987–6041, https://doi.org/10.1021/acs.chemrev.5b00603.

[34] L. Vivier, D. Duprez, Ceria-based solid catalysts for organic chemistry, ChemSusChem 3 (2010) 654–678, https://doi.org/10.1002/cssc.201000054.

[35] A. Trovarelli, Catalytic properties of ceria and CeO2-containing materials, Catal Rev. 38 (1996) 439–520, https://doi.org/10.1080/01614949608006464.

[36] A. Bueno - Lopez, K. Krishna, M. Makkee, J. Moulijn, Active oxygen from CeO2 and its role in catalysed soot oxidation, Catal. Lett. 99 (2005) 203–205, https://doi.org/10.1007/s10562-005-2120-x.

[37] M. Machida, Y. Murata, K. Kishikawa, D.J. Zhang, K. Ikeue, On the reasons for high activity of CeO2 catalyst for soot oxidation, Chem. Mater. 20 (2008) 4489–4494, https://doi.org/10.1021/Cm800832w.

[38] P. Fornasiero, G. Balducci, R. DiMonte, J. Kaspar, V. Sergo, G. Gubitosa, A. Ferrero, M. Graziani, Modification of the redox behaviour of CeO2 induced by structural doping with ZrO2, J. Catal. 164 (1996) 173–183, https://doi.org/10.1006/jcat.1996.0373.

[39] A. Trovarelli, Structural and oxygen storage/release properties of CeO2-based solid solutions, Comm. Inorg. Chem. 20 (1999) 263–284, https://doi.org/10.1080/02603599908021446.

[40] E. Aneggi, M. Boaro, C. de Leitenburg, G. Dolcetti, A. Trovarelli, Insights into the redox properties of ceria-based oxides and their implications in catalysis, J. Alloy. Compd. 408 (2006) 1096–1102, https://doi.org/10.1016/j.jallcom.2004.12.113.

[41] X. Huang, K. Zhang, B. Peng, G. Wang, M. Muhler, F. Wang, Ceria-based materials for thermocatalytic and photocatalytic organic synthesis, ACS Catal. 11 (2021) 9618–9678, https://doi.org/10.1021/acscatal.1c02443.

[42] E.S. Gore, Ruthenium catalysed oxidations of organic compounds, Platin. Metal. Rev. 27 (1983) 15.

[43] M. Pagliaro, S. Campestrini, R. Ciriminna, Ru-based oxidation catalysis, Chem. Soc. Rev. 34 (2005) 837–845, https://doi.org/10.1039/b507094p.

[44] T. Punniyamurthy, S. Velusamy, J. Iqbal, Recent advances in transition metal catalyzed oxidation of organic substrates with molecular oxygen, Chem. Rev. 105 (2005) 2329–2364, https://doi.org/10.1021/cr050523v.

[45] C. Bruneau, P. Dixneuf, I. Arends, Ruthenium Catalysts and Fine Chemistry, 2010.

[46] L. Pardatscher, B.J. Hofmann, P.J. Fischer, S.M. Holzl, R.M. Reich, F.E. Kuhn, W. Baratta, Highly efficient abnormal NHC ruthenium catalyst for oppenauer-type oxidation and transfer hydrogenation reactions, ACS Catal. 9 (2019) 11302–11306, https://doi.org/10.1021/acscatal.9b03677.

[47] R. Matheu, M.Z. Ertem, C. Gimbert-Suriñach, X. Sala, A. Llobet, Seven coordinated molecular ruthenium–water oxidation catalysts: a coordination chemistry journey, Chem. Rev. 119 (2019) 3453–3471, https://doi.org/10.1021/acs.chemrev.8b00537.

[48] S. Dey, G.C. Dhal, Applications of rhodium and ruthenium catalysts for CO oxidation: an overview, Polytechnica 3 (2020) 26–42, https://doi.org/10.1007/s41050-020-00023-5.

[49] R. Jenkins, R.L. Snyder, Introduction to X-ray Powder Diffractometry, Wiley, New York, 1996.

[50] R.A. Young, The Rietveld Method IUCr, Oxford University Press, New York., 1993.

[51] A.C. Larson, R.B. Von Dreele, General Structure Analysis System (GSAS), Los Alamos National Laboratory, 2000. Report LAUR 86-748.

[52] B.H. Toby, EXPGUI, a graphical user interface for GSAS, J. Appl. Crystallogr. 34 (2001) 210–213.

[53] D.R. Mullins, S.H. Overbury, D.R. Huntley, Electron spectroscopy of single crystal and polycrystalline cerium oxide surfaces, Surf. Sci. 409 (1998) 307–319, https://doi.org/10.1016/S0039-6028(98)00257-X.

[54] X. Qin, X. Chen, M. Chen, J. Zhang, H. He, C. Zhang, Highly efficient Ru/CeO2 catalysts for formaldehyde oxidation at low temperature and the mechanistic study, Catal. Sci. Technol. 11 (2021) 1914–1921, https://doi.org/10.1039/d0cy01894e.

[55] J.M. López, A.L. Gilbank, T. García, B. Solsona, S. Agouram, L. Torrente-Murciano, The prevalence of surface oxygen vacancies over the mobility of bulk oxygen in nanostructured ceria for the total toluene oxidation, Appl. Cataly. B: Environ. (2015) 403–412, https://doi.org/10.1016/j.apcatb.2015.03.017, 174-175.

[56] X. Garcia, L. Soler, N.J. Divins, X. Vendrell, I. Serrano, I. Lucentini, J. Prat, E. Solano, M. Tallarida, C. Escudero, J. Llorca, Ceria-based catalysts studied by near ambient pressure X-ray photoelectron spectroscopy: a review, Catalysts 10 (2020) 286, https://doi.org/10.3390/catal10030286.

[57] J. Kullgren, K. Hermansson, P. Broqvist, Supercharged low-temperature oxygen storage capacity of ceria at the nanoscale, J. Phys. Chem. Lett. 4 (2013) 604–608, https://doi.org/10.1021/jz3020524.

[58] J.H. Xu, J. Harmer, G.Q. Li, T. Chapman, P. Collier, S. Longworth, S.C. Tsang, Size dependent oxygen buffering capacity of ceria nanocrystals, Chem. Commun. 46 (2010) 1887–1889, https://doi.org/10.1039/b923780a.

[59] X. Garcia, L. Soler, A. Casanovas, C. Escudero, J. Llorca, X-ray photoelectron and Raman spectroscopy of nanostructured ceria in soot oxidation under operando conditions, Carbon N Y 178 (2021) 164–180, https://doi.org/10.1016/j.carbon.2021.03.009.

[60] F. Giordano, A. Trovarelli, C. de Leitenburg, M. Giona, A model for the temperature-programmed reduction of low and high surface area ceria, J. Catal. 193 (2000) 273–282, https://doi.org/10.1006/jcat.2000.2900.

[61] F. Fally, V. Perrichon, H. Vidal, J. Kaspar, G. Blanco, J.M. Pintado, S. Bernal, G. Colon, M. Daturi, J.C. Lavalley, Modification of the oxygen storage capacity of CeO2–ZrO2 mixed oxides after redox cycling aging, Catal. Today 59 (2000) 373–386, https://doi.org/10.1016/S0920-5861(00)00302-3.

[62] J. Shi, F. Hui, J. Yuan, Q. Yu, S. Mei, Q. Zhang, J. Li, W. Wang, J. Yang, J. Lu, Ru-Ti oxide based catalysts for HCl oxidation: the favorable oxygen species and influence of Ce additive, Catalysts 9 (2019) 108. ttps://doi.org/10.3390/catal9020108.

[63] J. Okal, M. Zawadzki, P. Kraszkiewicz, K. Adamska, Ru/CeO2 catalysts for combustion of mixture of light hydrocarbons: effect of preparation method and metal salt precursors, Appl. Catal. a-Gen. 549 (2018) 161–169, https://doi.org/10.1016/j.apcata.2017.09.036.

[64] S. Hosokawa, H. Kanai, K. Utani, Y. Taniguchi, Y. Saito, S. Imamura, State of Ru on CeO2 and its catalytic activity in the wet oxidation of acetic acid, Appl. Catal. B-Environ. 45 (2003) 181–187, https://doi.org/10.1016/S0926-3373(03)00129-2.

[65] S. Hosokawa, M. Taniguchi, K. Utani, H. Kanai, S. Imamura, Affinity order among noble metals and CeO2, Appl. Catal. a-Gen. 289 (2005) 115–120, https://doi.org/10.1016/j.apcata.2005.04.048.

[66] S. Aouad, E. Saab, E. Abi-Aad, A. Aboukais, Study of the Ru/Ce system in the oxidation of carbon black and volatile organic compounds, Kinet. Catal.+ 48 (2007) 835–840, https://doi.org/10.1134/S0023158407060122.

[67] S. Hosokawa, S. Nogawa, M. Taniguchi, K. Utani, H. Kanai, S. Imamura, Oxidation characteristics of Ru/CeO2 catalyst, Appl. Catal. a-Gen. 288 (2005) 67–73, https://doi.org/10.1016/j.apcata.2005.04.026.

[68] S. Hosokawa, Y. Hayashi, S. Imamura, K. Wada, M. Inoue, Effect of the preparation conditions of Ru/CeO2 catalysts for the liquid phase oxidation of benzyl alcohol, Catal. Lett. 129 (2009) 394–399, https://doi.org/10.1007/s10562-009-9845-x.

[69] L.J. Liu, Z.J. Yao, Y. Deng, F. Gao, B. Liu, L. Dong, Morphology and crystal-plane effects of nanoscale ceria on the activity of CuO/CeO2 for NO reduction by CO, ChemCatChem 3 (2011) 978–989, https://doi.org/10.1002/cctc.201000320.
[70] R.C.R. Neto, M. Schmal, Synthesis of CeO2 and CeZrO2 mixed oxide nanostructured catalysts for the iso-syntheses reaction, Appl. Cataly. A: Gener. 450 (2013) 131–142, https://doi.org/10.1016/j.apcata.2012.10.002.
[71] S. Loridant, Raman spectroscopy as a powerful tool to characterize ceria-based catalysts, Catal. Today 373 (2021) 98–111, https://doi.org/10.1016/j.cattod.2020.03.044.
[72] Y. Gu, X. Jiang, W. Sun, S. Bai, Q. Dai, X. Wang, 1,2-dichloroethane deep oxidation over bifunctional Ru/Ce x Al y catalysts, Acs Omega 3 (2018) 8460–8470, https://doi.org/10.1021/acsomega.8b00592.
[73] Z. Wang, Z. Huang, J.T. Brosnahan, S. Zhang, Y. Guo, Y. Guo, L. Wang, Y. Wang, W. Zhan, Ru/CeO2 catalyst with optimized CeO2 support morphology and surface facets for propane combustion, Environ. Sci. Technol. 53 (2019) 5349–5358, https://doi.org/10.1021/acs.est.9b01929.
[74] Z.L. Wu, M.J. Li, J. Howe, H.M. Meyer, S.H. Overbury, Probing defect sites on CeO2 nanocrystals with well-defined surface planes by Raman spectroscopy and O2 adsorption, Langmuir 26 (2010) 16595–16606, https://doi.org/10.1021/la101723w.
[75] H. Huang, J.H. Liu, P. Sun, S. Ye, Study on the simultaneous reduction of diesel engine soot and NO with nano-CeO2 catalysts, RSC Adv. 6 (2016) 102028–102034, https://doi.org/10.1039/c6ra23125j.
[76] S.Y. Mar, C.S. Chen, Y.S. Huang, K.K. Tiong, Characterization of Ruo2 thin-films by Raman-spectroscopy, Appl. Surf. Sci. 90 (1995) 497–504, https://doi.org/10.1016/0169-4332(95)00177-8.
[77] T. Taniguchi, T. Watanabe, N. Sugiyama, A.K. Subramani, H. Wagata, N. Matsushita, M. Yoshimura, Identifying defects in ceria-based nanocrystals by UV resonance raman spectroscopy, J. Phys. Chem. C 113 (2009) 19789–19793, https://doi.org/10.1021/jp9049457.
[78] J. Chen, Q.H. Zhang, Y. Wang, H.L. Wan, Size-dependent catalytic activity of supported palladium nanoparticles for aerobic oxidation of alcohols, Adv. Synth. Catal. 350 (2008) 453–464, https://doi.org/10.1002/adsc.200700350.
[79] J.P. Zhao, W.Y. Hernandez, W.J. Zhou, Y. Yang, E.I. Vovk, M. Capron, V. Ordomsky, Selective oxidation of alcohols to carbonyl compounds over small size colloidal Ru nanoparticles, ChemCatChem 12 (2020) 238–247, https://doi.org/10.1002/cctc.201901249.
[80] X. Li, J. Feng, M. Perdjon, R. Oh, W. Zhao, X. Huang, S. Liu, Investigations of supported Au-Pd nanoparticles on synthesized CeO2 with different morphologies and application in solvent-free benzyl alcohol oxidation, Appl. Surf. Sci. 505 (2020), 144473, https://doi.org/10.1016/j.apsusc.2019.144473.
[81] T. Li, F. Liu, Y. Tang, L. Li, S. Miao, Y. Su, J. Zhang, J. Huang, H. Sun, M. Haruta, A. Wang, B. Qiao, J. Li, T. Zhang, Maximizing the number of interfacial sites in single-atom catalysts for the highly selective, solvent-free oxidation of primary alcohols, Angew. Chemie Int. Ed. 57 (2018) 7795–7799, https://doi.org/10.1002/anie.201803272.
[82] E. Nowicka, S. Althahban, T.D. Leah, G. Shaw, D. Morgan, C.J. Kiely, A. Roldan, G. J. Hutchings, Benzyl alcohol oxidation with Pd-Zn/TiO2: computational and experimental studies, Sci. Technol. Adv. Mat. 20 (2019) 367–378, https://doi.org/10.1080/14686996.2019.1598237.
[83] Y.Y. Li, A. Sabbaghi, J.L. Huang, K.C. Li, L.S. Tsui, F.L.Y. Lam, X.J. Hu, Aerobic oxidation of benzyl alcohol: influence from catalysts basicity, acidity, and preparation methods, Mol. Catal. 485 (2020), 110789, https://doi.org/10.1016/J.Mcat.2020.110789.
[84] M.M. Du, G.N. Zeng, C.H. Ye, H. Jin, J.L. Huang, D.H. Sun, Q.B. Li, B. Chen, X.N. Li, Solvent-free photo-thermocatalytic oxidation of benzyl alcohol on Pd/TiO2(B) nanowires, Mol. Catal. 483 (2020), 110771, https://doi.org/10.1016/J.Mcat.2020.110771.
[85] H.M. Alshammari, J.R. Humaidi, M.S. Alhumaimess, O.F. Aldosari, M.H. Alotaibi, H.M.A. Hassan, I. Wawata, Bimetallic Au:Pd nanoparticle supported on MgO for the oxidation of benzyl alcohol, React. Kinet. Mech. Cat. 128 (2019) 97–108, https://doi.org/10.1007/s11144-019-01639-0.
[86] N.F. Zheng, G.D. Stucky, Promoting gold nanocatalysts in solvent-free selective aerobic oxidation of alcohols, Chem. Commun. (2007) 3862–3864, https://doi.org/10.1039/b706864f.
[87] D. Jung, S. Lee, K. Na, RuO2 supported NaY zeolite catalysts: effect of preparation methods on catalytic performance during aerobic oxidation of benzyl alcohol, Solid State Sci. 72 (2017) 150–155, https://doi.org/10.1016/j.solidstatesciences.2017.08.022.
[88] T. Yasu-eda, S. Kitamura, N.-o. Ikenaga, T. Miyake, T. Suzuki, Selective oxidation of alcohols with molecular oxygen over Ru/CaO–ZrO2 catalyst, J. Molecul. Cataly. A: Chem. 323 (2010) 7–15, https://doi.org/10.1016/j.molcata.2010.03.018.
[89] S. Hosokawa, Y. Hayashi, S. Imamura, K. Wada, M. Inoue, Effect of the preparation conditions of Ru/CeO2 catalysts for the liquid phase oxidation of benzyl alcohol, Catal. Lett. 129 (2009) 394–399, https://doi.org/10.1007/s10562-009-9845-x.
[90] Z. Ma, X. Xiong, C. Song, B. Hu, W. Zhang, Electronic metal–support interactions enhance the ammonia synthesis activity over ruthenium supported on Zr-modified CeO2 catalysts, RSC Adv. 6 (2016) 51106–51110, https://doi.org/10.1039/c6ra10540h.
[91] P. Bera, K.C. Patil, V. Jayaram, G.N. Subbanna, M.S. Hegde, Ionic dispersion of Pt and Pd on CeO2 by combustion method: effect of metal-ceria interaction on catalytic activities for NO reduction and CO and hydrocarbon oxidation, J. Catal. 196 (2000) 293–301, https://doi.org/10.1006/jcat.2000.3048.